

CERN-EP-2022-0811
2022/05/12

CMS-HIG-21-008

Search for Higgs boson decay to a charm quark-antiquark pair in proton-proton collisions at $\sqrt{s} = 13$ TeV

The CMS Collaboration

Abstract

A search for the standard model Higgs boson decaying to a charm quark-antiquark pair, $H \rightarrow c\bar{c}$, produced in association with a leptonically decaying V (W or Z) boson is presented. The search is performed with proton-proton collisions at $\sqrt{s} = 13$ TeV collected by the CMS experiment, corresponding to an integrated luminosity of 138 fb^{-1} . Novel charm jet identification and analysis methods using machine learning techniques are employed. The analysis is validated by searching for $Z \rightarrow c\bar{c}$ in VZ events, leading to its first observation at a hadron collider with a significance of 5.7 standard deviations. The observed (expected) upper limit on $\sigma(VH) \mathcal{B}(H \rightarrow c\bar{c})$ is $0.94 (0.50^{+0.22}_{-0.15}) \text{ pb}$ at 95% confidence level (CL), corresponding to 14 ($7.6^{+3.4}_{-2.3}$) times the standard model prediction. For the Higgs-charm Yukawa coupling modifier, κ_c , the observed (expected) 95% CL interval is $1.1 < |\kappa_c| < 5.5$ ($|\kappa_c| < 3.4$), the most stringent constraint to date.

Submitted to Physical Review Letters

The discovery of a Higgs boson (H) with the LHC Run 1 data by the ATLAS [1] and CMS [2, 3] experiments in 2012 was a major advance in the understanding of the electroweak (EW) symmetry breaking mechanism. The measured Higgs boson mass is 125.38 ± 0.14 GeV [4]. The observed interactions with gauge bosons and third-generation fermions [5–15], and all measured properties [4, 16–24], are compatible with standard model (SM) predictions. Recently, the CMS Collaboration reported the first evidence of Higgs boson decays to muons, i.e., second-generation leptons [25]. An important next milestone is the observation of its coupling to second-generation quarks. In this Letter, we focus on a search for Higgs boson decay to $c\bar{c}$, a charm quark-antiquark pair. The corresponding Yukawa coupling, y_c , can be significantly modified in the presence of physics beyond the SM [26–29]. However, the small branching ratio predicted by the SM, ubiquitous production of quark and gluon jets at the LHC, and the difficulty of identifying charm quark jets in a hadronic environment, including distinguishing them from bottom quark jets, make this a challenging measurement. Searches for $H \rightarrow c\bar{c}$ reported in Refs. [30–32] by the ATLAS and CMS Collaborations target the associated production of a Higgs boson with a V (W or Z) boson. Using 139 fb^{-1} of data at 13 TeV, the most recent search by the ATLAS Collaboration obtains an observed (expected) upper limit on the product of the production cross section $\sigma(\text{VH})$ and branching fraction $\mathcal{B}(H \rightarrow c\bar{c})$ of 26 (31) times the SM prediction at 95% confidence level (CL) [32].

This Letter presents a search for $H \rightarrow c\bar{c}$ in VH production using proton-proton (pp) collision data at $\sqrt{s} = 13$ TeV, collected by the CMS detector in 2016–2018, and corresponding to an integrated luminosity of 138 fb^{-1} [33–35]. Building upon a previous analysis by the CMS Collaboration [31], advanced c jet reconstruction and identification algorithms and sophisticated analysis techniques using machine learning (ML) have been further developed to significantly improve sensitivity.

The CMS apparatus [36] is a multipurpose, nearly hermetic detector, designed to trigger on [37, 38] and identify electrons, muons, photons, and (charged and neutral) hadrons [39–41]. A global reconstruction “particle-flow” (PF) algorithm [42] combines the information provided by the all-silicon inner tracker and by the crystal electromagnetic and brass-scintillator hadron calorimeters, operating inside a 3.8 T superconducting solenoid, with data from gas-ionization muon detectors embedded in the solenoid flux-return yoke, to reconstruct charged and neutral hadrons, electrons, photons, and muons (PF candidates) and build τ leptons, jets, missing transverse momentum, and other physics objects [43–45].

Two collections of jets, formed by PF candidates clustered using the anti- k_T algorithm [46, 47], are used in the search. The first uses a distance parameter $R = 0.4$, and will be referred to as “small- R ” jets. The second uses $R = 1.5$ and contains what are referred to as “large- R ” jets. The impact of particles from additional pp interactions within the same or nearby bunch crossings (pileup) is mitigated via the charged hadron subtraction algorithm [42] for small- R jets, and via the PUPPI [48, 49] algorithm for large- R jets. A regression algorithm [50] is developed to improve large- R jet mass reconstruction that exploits properties of the PF candidates and secondary vertices associated to the jet using the PARTICLENET graph neural network [51]. Mass resolution is improved by about 50% over traditional jet grooming algorithms [52, 53]. The small- R (large- R) jets are required to have transverse momentum (p_T) above 25 (200) GeV and to be within the tracker acceptance.

Signal and background processes are simulated using various Monte Carlo event generators. The detector response is modeled with GEANT4 [54]. The WH and quark-induced ZH signal processes are generated at next-to-leading order (NLO) accuracy in quantum chromodynamics (QCD) using the POWHEG v2 [55–57] event generator extended with the multi-scale improved

NLO (MiNLO) procedure [58, 59], while the gluon-induced ZH process is generated at leading order (LO) accuracy with POWHEG v2. The Higgs boson mass is set to 125 GeV for all simulations. The production cross sections of the signal processes [60] are corrected as a function of $p_T(V)$ to next-to-next-to-leading order (NNLO) QCD + NLO EW accuracy combining the VHNNLO [61–64], VH@NNLO [65, 66], and HAWK v2.0 [67] generators, as described in Ref. [60].

The V+jets background samples are generated with MADGRAPH5_aMC@NLO v2.6.0 [68] at NLO with up to two additional partons. The top quark pair ($t\bar{t}$) [69] and single top quark production processes [70–72] are generated to NLO accuracy with POWHEG v2. The production cross sections for the $t\bar{t}$ samples are scaled to the NNLO prediction with the next-to-next-to-leading logarithmic resummation result obtained from TOP++ v2.0 [73], and the differential cross sections as a function of top quark p_T are corrected to the NNLO QCD + NLO EW prediction [74]. Diboson backgrounds are generated at NLO with POWHEG v2 (MADGRAPH5_aMC@NLO v2.4.2) for the WW [75] (WZ and ZZ) process. Production cross sections of the diboson processes are reweighted as a function of the subleading vector boson p_T to NNLO QCD + NLO EW accuracy [76].

The NLO NNPDF3.0 [77] (NNLO NNPDF3.1 [78]) parton distribution function (PDF) set is used for the 2016 (2017 and 2018) simulations. For parton showering and hadronization, including the $H \rightarrow c\bar{c}$ decay, matrix element generators are interfaced with PYTHIA v8.230 [79] with the CUETP8M1 [80] (CP5 [81]) underlying event tune for 2016 (2017 and 2018) samples. The matching of jets from matrix element calculations and those from parton showers is done with the FxFx [82] (MLM [83]) prescription for NLO (LO) samples. For all samples, pileup interactions are simulated with PYTHIA and added to the hard-scattering process. Events are then reweighted to match the pileup profile observed in data.

The analysis is carried out in mutually exclusive channels targeting leptonic decays of the vector bosons: $Z \rightarrow \nu\nu$, $W \rightarrow \ell\nu$, and $Z \rightarrow \ell\ell$, where ℓ is an electron or a muon, and referred to as the 0L, 1L, and 2L channels. Events are collected using triggers based on large missing transverse momentum, or the presence of one, or two well-identified and isolated leptons. The event selection criteria are detailed in Ref. [31].

As for the previous search [31], the analysis reconstructs the Higgs boson candidate (H_{cand}) assuming either a “merged-jet” topology, in which the hadronization products of the two charm quarks are reconstructed as a single large- R jet, or a “resolved-jet” topology, in which the H_{cand} is reconstructed from two well-separated and individually resolved small- R c jets. These two topologies can have significant overlap and are made distinct in reference to whether a given H_{cand} , identified through a large- R jet in the event, has p_T above or below a threshold of 300 GeV for the definition of the merged-jet and the resolved-jet topology, respectively, where the dividing line is chosen to maximize sensitivity to $VH(H \rightarrow c\bar{c})$.

On average, the H_{cand} large- R jets in the signal process have larger p_T than those from the V+jets and $t\bar{t}$ backgrounds. Thus, the high- p_T regime explored in the merged-jet topology, although amounting to less than 5% of the signal cross section, provides significant sensitivity to the search. Because the highly boosted Higgs boson decay produces a more narrowly concentrated collection of final-state particles, the use of a single large- R jet enhances the probability of correctly capturing the hadronization products of both charm quarks, and facilitates the accounting of final-state radiation (FSR) emitted by the quarks. A detailed discussion of the advantages can be found in Refs. [31, 53, 84].

State-of-the-art performance in the reconstruction and identification of the pair of c quarks from the Higgs boson decay is achieved with PARTICLENET [51], a novel jet identification algorithm.

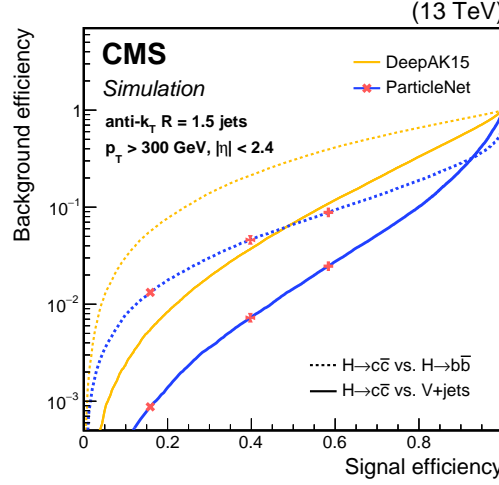


Figure 1: Performance of PARTICLENET (blue lines) for identifying a $c\bar{c}$ pair for large- R jets with $p_T > 300$ GeV. The solid (dashed) line shows the efficiency to correctly identify $H \rightarrow c\bar{c}$ vs. the efficiency of misidentifying quarks or gluons from the V +jets process (vs. $H \rightarrow b\bar{b}$). The red crosses represent the three working points used in the merged-jet analysis. The performance of DEEPAK15 (yellow lines) used in Ref. [31] is shown for comparison.

Using PF candidates and secondary vertices associated to large- R jets as inputs, PARTICLENET simultaneously exploits information related to jet substructure, flavor, and pileup with a graph neural network [85], yielding substantial gains over other approaches [86, 87]. Decorrelation of the algorithm’s response with the jet mass is achieved by training it with a dedicated set of simulations produced with the same jet mass distributions for the signal and background processes [86]. Figure 1 shows the performance of the $c\bar{c}$ discriminant in identifying a pair of c quarks from Higgs boson decay for large- R jets with $p_T > 300$ GeV. PARTICLENET is compared to the previous state-of-the-art $c\bar{c}$ discriminant “DEEPAK15” [31, 88], yielding an improvement by a factor of 4 to 7 in the rejection of other jet flavors. Three working points are defined on the $c\bar{c}$ discriminant distribution with approximately 58, 40, and 16% efficiencies for identifying a $c\bar{c}$ pair. The corresponding misidentification rates of light quark and gluon jets ($b\bar{b}$ jets) are 2 (9), 0.7 (5), and 0.08 (1)%. These working points are used to separate events into three mutually exclusive categories with different $c\bar{c}$ purity to improve the sensitivity of the analysis. The $c\bar{c}$ identification efficiency in data is measured using a sample of events containing a gluon splitting to $c\bar{c}$. To increase the similarity to $H \rightarrow c\bar{c}$ decay, a dedicated BDT classifier is developed to enrich jets where a large fraction of momentum is carried by the quark pair from gluon splitting rather than by additionally radiated gluons [89]. The p_T -dependent data-to-simulation efficiency ratios (used as corrective scale factors) are typically 0.9–1.3 with corresponding uncertainties of 20–30%.

The main backgrounds, $t\bar{t}$ and V +jets, are suppressed by a separate boosted decision tree (BDT) classifier for each channel, using kinematical variables that are not correlated with the H_{cand} mass, $m(H_{\text{cand}})$, or the $c\bar{c}$ discriminant as inputs. The BDT design relies on previous developments [31] with improvements in variable selection and training procedure, leading to $\approx 15\%$ enhancement of the sensitivity of the analysis. The BDT discriminants are used to define 2 (1) signal regions (SRs) in the 1L (0L and 2L) channel. Events in the SRs are further subdivided into the three $c\bar{c}$ discriminant categories mentioned above. The $m(H_{\text{cand}})$ distributions are used to separate signal and background contributions in each SR, as both the BDTs and the $c\bar{c}$ discriminant are designed to be largely independent of $m(H_{\text{cand}})$.

More than 95% of the VH events have a Higgs boson with $p_T(H) < 300$ GeV, corresponding to the phase space region where the Higgs boson decay products generally give rise to two distinctly reconstructed small- R jets. The resolved-jet topology exploits a large fraction of this phase space, which, however, contains higher background contamination than that used in the merged-jet analysis. The H_{cand} is reconstructed via two distinct small- R jets. The identification of c jets relies on the ML-based DEEPJET algorithm [90, 91]. The discrimination between c jets and light quark or gluon jets (b jets) is achieved via the ratio of the corresponding probabilities, defined as $CvsL$ ($CvsB$) [92]. Potential differences in the discriminant shapes between data and simulation are taken into account by flavor-dependent simulation-to-data efficiency scale factors [92], which are typically in the 0.9–1.0 range. The corresponding uncertainties range from $\approx 2\%$ for light quark and gluon jets or b jets, to $\approx 5\%$ for c jets.

The two jets with the highest $CvsL$ discriminants in each event are selected to reconstruct the H_{cand} momentum four-vector. To improve sample purity, criteria are imposed on $CvsL$ and $CvsB$ for the leading jet that correspond to $\approx 40\%$ c jet efficiency, for ≈ 4 (≈ 16)% light quark or gluon jet (b jet) misidentification rate. Multiple corrections are applied to improve the $m(H_{\text{cand}})$ reconstruction. To account for a potential underestimation of the c jet energy, due to the presence of undetected neutrinos in c hadron decays, an ML-based jet energy regression algorithm [93], originally developed for b jets, is adapted for c jets. In addition, small- R jets reconstructed in the vicinity of H_{cand} jets, often stemming from FSR, are included in the H_{cand} reconstruction [31]. The $m(H_{\text{cand}})$ resolution in the 2L channel is further improved via a kinematic fit by balancing the momenta of the two small- R jets and the lepton pair within experimental uncertainties [94]. These steps improve the $m(H_{\text{cand}})$ resolution up to 20%. Finally, a BDT classifier is developed to maximize the discrimination power between signal and background processes in each channel, using event-level kinematical variables, c jet identification discriminants, and properties of H_{cand} , including $m(H_{\text{cand}})$, as inputs [31].

The signal strength modifier μ , defined as $(\sigma\mathcal{B})_{\text{obs}} / (\sigma\mathcal{B})_{\text{SM}}$ where σ is the signal production cross section and \mathcal{B} is the branching fraction, is measured via a binned maximum likelihood fit to data. The best-fit value of μ and an approximate 68% CL confidence interval are extracted following the procedure in Ref. [17]. The fitted variable is $m(H_{\text{cand}})$ in the merged-jet analysis, and the BDT discriminant in the resolved-jet analysis. The normalizations of the main backgrounds, namely V +jets and $t\bar{t}$, are estimated by including dedicated control regions in the fit following the strategy detailed in Ref. [31]. Contributions from single top, diboson and $VH(H \rightarrow b\bar{b})$ processes are estimated from simulation assuming SM production rates. Because of improvements in c jet identification, the difficult $VH(H \rightarrow b\bar{b})$ background contribution in the high $c\bar{c}$ purity SRs is reduced from about twenty times to only about twice that expected for $VH(H \rightarrow c\bar{c})$, and the $VZ(Z \rightarrow b\bar{b})$ yield is reduced from more than 100% to about 10% of that expected for $VZ(Z \rightarrow c\bar{c})$. Contributions from $H \rightarrow \tau\tau$ decays are negligible after the above-mentioned selection criteria, and are not considered.

Systematic uncertainties affecting normalizations and shapes of fitted variables are taken into account via nuisance parameters. The relative contribution of each uncertainty source to the total uncertainty in the fitted μ is summarized in Table 1. The leading uncertainty is statistical because of the limited number of events in the SRs as well as the control regions used to extract background normalizations. The main experimental systematic uncertainties are associated with limited simulation sample sizes, particularly due to large fractions of negatively weighted events in the NLO V +jets samples, and the c jet identification efficiencies, representing ≈ 37 and $\approx 23\%$ of the total, respectively. Theoretical uncertainties in the cross sections, p_T spectra, PDFs, renormalization and factorization scales, represent $\approx 22\%$ of the total uncertainty in μ .

Table 1: The relative contributions to the total uncertainty in the signal strength modifier μ for the $VH(H \rightarrow c\bar{c})$ process, where the best fit is $\mu_{VH(H \rightarrow c\bar{c})} = 7.7^{+3.8}_{-3.5}$.

Uncertainty source	$\Delta\mu / (\Delta\mu)_{\text{tot}}$
Statistical	85%
Background normalizations	37%
Experimental	48%
Sizes of the simulated samples	37%
c jet identification efficiencies	23%
Jet energy scale and resolution	15%
Simulation modeling	11%
Integrated luminosity	6%
Lepton identification efficiencies	4%
Theory	22%
Backgrounds	17%
Signal	15%

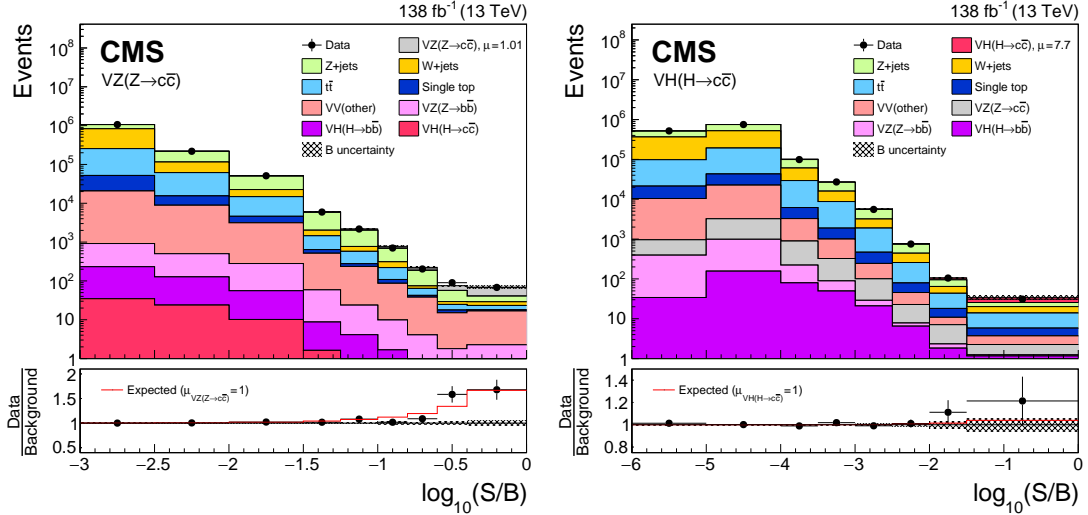


Figure 2: Distribution of events as a function of S/B in the $VZ(Z \rightarrow c\bar{c})$ (left) and $VH(H \rightarrow c\bar{c})$ (right) searches, where S and B are the postfit signal and background yields, respectively, in each bin of the fitted $m(H_{\text{cand}})$ or BDT discriminant distributions. The bottom panel shows the ratio of data to the total background, with the uncertainty in background indicated by gray hatching. The red line represents background plus SM signal divided by background.

A search for the analogous SM process $VZ(Z \rightarrow c\bar{c})$ is performed to validate the analysis strategy. The BDTs in the resolved-jet topology are modified by training them with $VZ(Z \rightarrow c\bar{c})$ as signal. No modification is needed for the BDTs in the merged-jet topology as they are independent of $m(H_{\text{cand}})$. The best fit μ of this process is $\mu_{VZ(Z \rightarrow c\bar{c})} = 1.01^{+0.23}_{-0.21}$, in agreement with the SM expectation. Figure 2 (left) shows the distribution of events in all channels, sorted into bins of similar signal-to-background ratios. The observed data shows a visible excess over the expected backgrounds. The significance of the excess is computed using the asymptotic distribution of a test statistic based on the profile likelihood ratio [95, 96]. The observed (expected) significance is 4.4 (4.7) standard deviations for the merged-jet analysis, 3.1 (3.3) standard deviations for the resolved-jet analysis, and 5.7 (5.9) standard deviations for their combination. This is the first observation of $Z \rightarrow c\bar{c}$ at a hadron collider.

Figure 2 (right) compares the observed data to the SM prediction in the search of $VH(H \rightarrow c\bar{c})$,

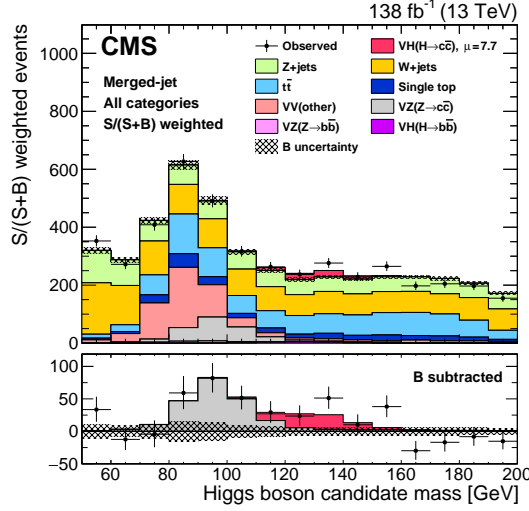


Figure 3: Combined $m(H_{\text{cand}})$ distribution in all channels of the merged-jet analysis. The fitted $m(H_{\text{cand}})$ distribution in each SR is weighted by $S/(S+B)$, where S and B are the postfit $VH(H \rightarrow c\bar{c})$ signal and total background yields. The lower panel shows data (points) and the fitted $VH(H \rightarrow c\bar{c})$ (red) and $VZ(Z \rightarrow c\bar{c})$ (grey) distributions after subtracting all other processes. Error bars represent pre-subtraction statistical uncertainties in data, while the gray hatching indicates the total uncertainty in the signal and all background processes.

where the best fit is $\mu_{VH(H \rightarrow c\bar{c})} = 7.7^{+3.8}_{-3.5}$. The fitted $m(H_{\text{cand}})$ distribution in the merged-jet topology is displayed in Fig. 3. No significant excess over the background-only hypothesis is observed. An upper limit on $\mu_{VH(H \rightarrow c\bar{c})}$ is extracted using the CL_s criterion [97, 98]. The test statistic is the profile likelihood ratio modified for upper limits [95], and the asymptotic approximation [96] is used in the limit setting procedure. The observed (expected) 95% CL upper limit on $\mu_{VH(H \rightarrow c\bar{c})}$ is 14 ($7.6^{+3.4}_{-2.3}$), which is equivalent to an observed (expected) upper limit on $\sigma(VH) \mathcal{B}(H \rightarrow c\bar{c})$ of 0.94 ($0.50^{+0.22}_{-0.15}$) pb. Contributions from the individual channels are summarized in Fig. 4. Tabulated results are provided in the HEPData record for this analysis [99].

The result is interpreted in the κ -framework [60, 100] by reparameterizing $\mu_{VH(H \rightarrow c\bar{c})}$ in terms of the Higgs-charm Yukawa coupling modifier κ_c , assuming only the Higgs boson decay widths are altered:

$$\mu_{VH(H \rightarrow c\bar{c})} = \frac{\kappa_c^2}{1 + \mathcal{B}_{\text{SM}}(H \rightarrow c\bar{c}) (\kappa_c^2 - 1)}. \quad (1)$$

The observed 95% CL interval is $1.1 < |\kappa_c| < 5.5$, and the corresponding expected constraint is $|\kappa_c| < 3.4$.

In summary, a search for the SM Higgs boson decaying to a pair of charm quarks in the CMS experiment is presented. Novel jet reconstruction and identification tools, and analysis techniques are developed for this analysis, which is validated by measuring the $VZ(Z \rightarrow c\bar{c})$ process. The observed Z boson signal relative to the SM prediction is $\mu_{VZ(Z \rightarrow c\bar{c})} = 1.01^{+0.23}_{-0.21}$, with an observed (expected) significance of 5.7 (5.9) standard deviations above the background-only hypothesis. This is the first observation of $Z \rightarrow c\bar{c}$ at a hadronic collider.

The observed (expected) upper limit on $\sigma(VH) \mathcal{B}(H \rightarrow c\bar{c})$ is 0.94 ($0.50^{+0.22}_{-0.15}$) pb, corresponding to 14 ($7.6^{+3.4}_{-2.3}$) times the theoretical prediction for an SM Higgs boson mass of 125.38 GeV. The observed (expected) 95% CL interval on the modifier, κ_c , for the Yukawa coupling of the Higgs boson to the charm quark is $1.1 < |\kappa_c| < 5.5$ ($|\kappa_c| < 3.4$). This is the most stringent constraint on κ_c to date.

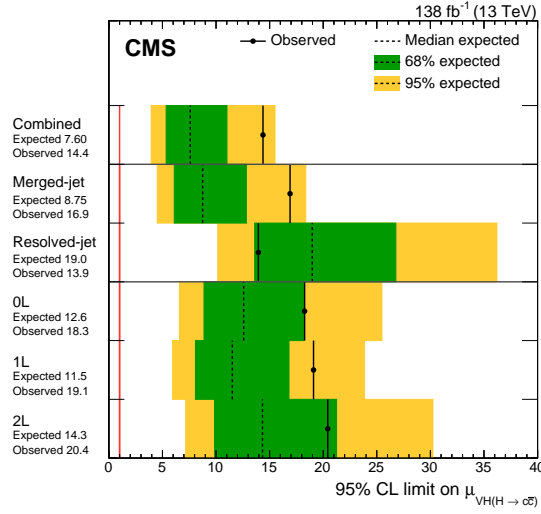


Figure 4: The 95% CL upper limits on $\mu_{VH(H \rightarrow c\bar{c})}$. Green and yellow bands indicate the 68 and 95% intervals on the expected limits, respectively. The vertical red line indicates the SM value $\mu_{VH(H \rightarrow c\bar{c})} = 1$.

References

- [1] ATLAS Collaboration, “Observation of a new particle in the search for the standard model Higgs boson with the ATLAS detector at the LHC”, *Phys. Lett. B* **716** (2012) 1, doi:10.1016/j.physletb.2012.08.020, arXiv:1207.7214.
- [2] CMS Collaboration, “Observation of a new boson at a mass of 125 GeV with the CMS experiment at the LHC”, *Phys. Lett. B* **716** (2012) 30, doi:10.1016/j.physletb.2012.08.021, arXiv:1207.7235.
- [3] CMS Collaboration, “Observation of a new boson with mass near 125 GeV in pp collisions at $\sqrt{s} = 7$ and 8 TeV”, *JHEP* **06** (2013) 081, doi:10.1007/JHEP06(2013)081, arXiv:1303.4571.
- [4] CMS Collaboration, “A measurement of the Higgs boson mass in the diphoton decay channel”, *Phys. Lett. B* **805** (2020) 135425, doi:10.1016/j.physletb.2020.135425, arXiv:2002.06398.
- [5] ATLAS Collaboration, “Measurement of Higgs boson production in the diphoton decay channel in pp collisions at center-of-mass energies of 7 and 8 TeV with the ATLAS detector”, *Phys. Rev. D* **90** (2014) 112015, doi:10.1103/PhysRevD.90.112015, arXiv:1408.7084.
- [6] CMS Collaboration, “Observation of the diphoton decay of the Higgs boson and measurement of its properties”, *Eur. Phys. J. C* **74** (2014) 3076, doi:10.1140/epjc/s10052-014-3076-z, arXiv:1407.0558.
- [7] ATLAS Collaboration, “Measurements of Higgs boson production and couplings in the four-lepton channel in pp collisions at center-of-mass energies of 7 and 8 TeV with the ATLAS detector”, *Phys. Rev. D* **91** (2015) 012006, doi:10.1103/PhysRevD.91.012006, arXiv:1408.5191.
- [8] CMS Collaboration, “Measurement of the properties of a Higgs boson in the four-lepton final state”, *Phys. Rev. D* **89** (2014) 092007, doi:10.1103/PhysRevD.89.092007, arXiv:1312.5353.

-
- [9] ATLAS Collaboration, “Observation and measurement of Higgs boson decays to WW^* with the ATLAS detector”, *Phys. Rev. D* **92** (2015) 012006, doi:10.1103/PhysRevD.92.012006, arXiv:1412.2641.
- [10] ATLAS Collaboration, “Study of $(W/Z)H$ production and Higgs boson couplings using $H \rightarrow WW^*$ decays with the ATLAS detector”, *JHEP* **08** (2015) 137, doi:10.1007/JHEP08(2015)137, arXiv:1506.06641.
- [11] CMS Collaboration, “Measurement of Higgs boson production and properties in the WW decay channel with leptonic final states”, *JHEP* **01** (2014) 096, doi:10.1007/JHEP01(2014)096, arXiv:1312.1129.
- [12] ATLAS Collaboration, “Evidence for the Higgs-boson Yukawa coupling to tau leptons with the ATLAS detector”, *JHEP* **04** (2015) 117, doi:10.1007/JHEP04(2015)117, arXiv:1501.04943.
- [13] CMS Collaboration, “Evidence for the 125 GeV Higgs boson decaying to a pair of τ leptons”, *JHEP* **05** (2014) 104, doi:10.1007/JHEP05(2014)104, arXiv:1401.5041.
- [14] CMS Collaboration, “Observation of the Higgs boson decay to a pair of tau leptons”, *Phys. Lett. B* **779** (2017) 283, doi:10.1016/j.physletb.2018.02.004, arXiv:1708.00373.
- [15] CMS Collaboration, “Measurements of properties of the Higgs boson decaying to a W boson pair in pp collisions at $\sqrt{s} = 13$ TeV”, *Phys. Lett. B* **791** (2019) 96, doi:10.1016/j.physletb.2018.12.073, arXiv:1806.05246.
- [16] ATLAS Collaboration, “Measurements of the Higgs boson production and decay rates and coupling strengths using pp collision data at $\sqrt{s} = 7$ and 8 TeV in the ATLAS experiment”, *Eur. Phys. J. C* **76** (2016) 6, doi:10.1140/epjc/s10052-015-3769-y, arXiv:1507.04548.
- [17] CMS Collaboration, “Precise determination of the mass of the Higgs boson and tests of compatibility of its couplings with the standard model predictions using proton collisions at 7 and 8 TeV”, *Eur. Phys. J. C* **75** (2015) 212, doi:10.1140/epjc/s10052-015-3351-7, arXiv:1412.8662.
- [18] CMS Collaboration, “Study of the mass and spin-parity of the Higgs boson candidate via its decays to Z boson pairs”, *Phys. Rev. Lett.* **110** (2013) 081803, doi:10.1103/PhysRevLett.110.081803, arXiv:1212.6639.
- [19] ATLAS Collaboration, “Evidence for the spin-0 nature of the Higgs boson using ATLAS data”, *Phys. Lett. B* **726** (2013) 120, doi:10.1016/j.physletb.2013.08.026, arXiv:1307.1432.
- [20] ATLAS and CMS Collaborations, “Measurements of the Higgs boson production and decay rates and constraints on its couplings from a combined ATLAS and CMS analysis of the LHC pp collision data at $\sqrt{s} = 7$ and 8 TeV”, *JHEP* **08** (2016) 045, doi:10.1007/JHEP08(2016)045, arXiv:1606.02266.
- [21] ATLAS and CMS Collaborations, “Combined measurement of the Higgs boson mass in pp collisions at $\sqrt{s} = 7$ and 8 TeV with the ATLAS and CMS experiments”, *Phys. Rev. Lett.* **114** (2015) 191803, doi:10.1103/PhysRevLett.114.191803, arXiv:1503.07589.

- [22] CMS Collaboration, “Measurements of properties of the Higgs boson decaying into the four-lepton final state in pp collisions at $\sqrt{s} = 13$ TeV”, *JHEP* **11** (2017) 047, doi:10.1007/JHEP11(2017)047, arXiv:1706.09936.
- [23] ATLAS Collaboration, “Combined measurement of differential and total cross sections in the $H \rightarrow \gamma\gamma$ and the $H \rightarrow ZZ^* \rightarrow 4\ell$ decay channels at $\sqrt{s} = 13$ TeV with the ATLAS detector”, *Phys. Lett. B* **786** (2018) 114, doi:10.1016/j.physletb.2018.09.019, arXiv:1805.10197.
- [24] ATLAS Collaboration, “Measurement of the Higgs boson mass in the $H \rightarrow ZZ^* \rightarrow 4\ell$ and $H \rightarrow \gamma\gamma$ channels with $\sqrt{s} = 13$ TeV pp collisions using the ATLAS detector”, *Phys. Lett. B* **784** (2018) 345, doi:10.1016/j.physletb.2018.07.050, arXiv:1806.00242.
- [25] CMS Collaboration, “Search for the Higgs boson decaying to two muons in proton-proton collisions at $\sqrt{s} = 13$ TeV”, *Phys. Rev. Lett.* **122** (2019) 021801, doi:10.1103/PhysRevLett.122.021801, arXiv:1807.06325.
- [26] D. Ghosh, R. S. Gupta, and G. Perez, “Is the Higgs mechanism of fermion mass generation a fact? A Yukawa-less first-two-generation model”, *Phys. Lett. B* **755** (2016) 504, doi:10.1016/j.physletb.2016.02.059, arXiv:1508.01501.
- [27] F. J. Botella, G. C. Branco, M. N. Rebelo, and J. I. Silva-Marcos, “What if the masses of the first two quark families are not generated by the standard model Higgs boson?”, *Phys. Rev. D* **94** (2016) 115031, doi:10.1103/PhysRevD.94.115031, arXiv:1602.08011.
- [28] R. Harnik, J. Kopp, and J. Zupan, “Flavor violating Higgs decays”, *JHEP* **03** (2013) 026, doi:10.1007/JHEP03(2013)026, arXiv:1209.1397.
- [29] W. Altmannshofer et al., “Collider signatures of flavorful Higgs bosons”, *Phys. Rev. D* **94** (2016) 115032, doi:10.1103/PhysRevD.94.115032, arXiv:1610.02398.
- [30] ATLAS Collaboration, “Search for the decay of the Higgs boson to charm quarks with the ATLAS experiment”, *Phys. Rev. Lett.* **120** (2018) 211802, doi:10.1103/PhysRevLett.120.211802, arXiv:1802.04329.
- [31] CMS Collaboration, “A search for the standard model Higgs boson decaying to charm quarks”, *JHEP* **03** (2020) 131, doi:10.1007/JHEP03(2020)131, arXiv:1912.01662.
- [32] ATLAS Collaboration, “Direct constraint on the Higgs-charm coupling from a search for Higgs boson decays into charm quarks with the ATLAS detector”, 2022. arXiv:2201.11428. Submitted to *EPJC*.
- [33] CMS Collaboration, “Precision luminosity measurement in proton-proton collisions at $\sqrt{s} = 13$ TeV in 2015 and 2016 at CMS”, *Eur. Phys. J. C* **81** (2021) 800, doi:10.1140/epjc/s10052-021-09538-2, arXiv:2104.01927.
- [34] CMS Collaboration, “CMS luminosity measurement for the 2017 data-taking period at $\sqrt{s} = 13$ TeV”, CMS Physics Analysis Summary CMS-PAS-LUM-17-004, 2018.
- [35] CMS Collaboration, “CMS luminosity measurement for the 2018 data-taking period at $\sqrt{s} = 13$ TeV”, CMS Physics Analysis Summary CMS-PAS-LUM-18-002, 2019.

-
- [36] CMS Collaboration, “The CMS experiment at the CERN LHC”, *JINST* **3** (2008) S08004, doi:10.1088/1748-0221/3/08/S08004.
- [37] CMS Collaboration, “Performance of the CMS Level-1 trigger in proton-proton collisions at $\sqrt{s} = 13$ TeV”, *JINST* **15** (2020) P10017, doi:10.1088/1748-0221/15/10/P10017, arXiv:2006.10165.
- [38] CMS Collaboration, “The CMS trigger system”, *JINST* **12** (2017) P01020, doi:10.1088/1748-0221/12/01/P01020, arXiv:1609.02366.
- [39] CMS Collaboration, “Electron and photon reconstruction and identification with the CMS experiment at the CERN LHC”, *JINST* **16** (2021) P05014, doi:10.1088/1748-0221/16/05/P05014, arXiv:2012.06888.
- [40] CMS Collaboration, “Performance of the CMS muon detector and muon reconstruction with proton-proton collisions at $\sqrt{s} = 13$ TeV”, *JINST* **13** (2018) P06015, doi:10.1088/1748-0221/13/06/P06015, arXiv:1804.04528.
- [41] CMS Collaboration, “Description and performance of track and primary-vertex reconstruction with the CMS tracker”, *JINST* **9** (2014) P10009, doi:10.1088/1748-0221/9/10/P10009, arXiv:1405.6569.
- [42] CMS Collaboration, “Particle-flow reconstruction and global event description with the CMS detector”, *JINST* **12** (2017) P10003, doi:10.1088/1748-0221/12/10/P10003, arXiv:1706.04965.
- [43] CMS Collaboration, “Performance of reconstruction and identification of τ leptons decaying to hadrons and ν_τ in pp collisions at $\sqrt{s} = 13$ TeV”, *JINST* **13** (2018) P10005, doi:10.1088/1748-0221/13/10/P10005, arXiv:1809.02816.
- [44] CMS Collaboration, “Jet energy scale and resolution in the CMS experiment in pp collisions at 8 TeV”, *JINST* **12** (2017) P02014, doi:10.1088/1748-0221/12/02/P02014, arXiv:1607.03663.
- [45] CMS Collaboration, “Performance of missing transverse momentum reconstruction in proton-proton collisions at $\sqrt{s} = 13$ TeV using the CMS detector”, *JINST* **14** (2019) P07004, doi:10.1088/1748-0221/14/07/P07004, arXiv:1903.06078.
- [46] M. Cacciari, G. P. Salam, and G. Soyez, “The anti- k_T jet clustering algorithm”, *JHEP* **04** (2008) 063, doi:10.1088/1126-6708/2008/04/063, arXiv:0802.1189.
- [47] M. Cacciari, G. P. Salam, and G. Soyez, “FastJet user manual”, *Eur. Phys. J. C* **72** (2012) 1896, doi:10.1140/epjc/s10052-012-1896-2, arXiv:1111.6097.
- [48] CMS Collaboration, “Pileup mitigation at CMS in 13 TeV data”, *JINST* **15** (2020) P09018, doi:10.1088/1748-0221/15/09/P09018, arXiv:2003.00503.
- [49] D. Bertolini, P. Harris, M. Low, and N. Tran, “Pileup per particle identification”, *JHEP* **10** (2014) 059, doi:10.1007/JHEP10(2014)059, arXiv:1407.6013.
- [50] CMS Collaboration, “Mass regression of highly-boosted jets using graph neural networks”, CMS Detector Performance Note CMS-DP-2021-017, 2021.
- [51] H. Qu and L. Gouskos, “Jet tagging via particle clouds”, *Phys. Rev. D* **101** (2020) 056019, doi:10.1103/PhysRevD.101.056019, arXiv:1902.08570.

- [52] M. Dasgupta, A. Fregoso, S. Marzani, and G. P. Salam, “Towards an understanding of jet substructure”, *JHEP* **09** (2013) 029, doi:10.1007/JHEP09(2013)029, arXiv:1307.0007.
- [53] J. M. Butterworth, A. R. Davison, M. Rubin, and G. P. Salam, “Jet substructure as a new Higgs search channel at the LHC”, *Phys. Rev. Lett.* **100** (2008) 242001, doi:10.1103/PhysRevLett.100.242001, arXiv:0802.2470.
- [54] GEANT4 Collaboration, “GEANT4 — A simulation toolkit”, *Nucl. Instrum. Meth. A* **506** (2003) 250, doi:10.1016/S0168-9002(03)01368-8.
- [55] P. Nason, “A new method for combining NLO QCD with shower Monte Carlo algorithms”, *JHEP* **11** (2004) 040, doi:10.1088/1126-6708/2004/11/040, arXiv:hep-ph/0409146.
- [56] S. Frixione, P. Nason, and C. Oleari, “Matching NLO QCD computations with parton shower simulations: the POWHEG method”, *JHEP* **11** (2007) 070, doi:10.1088/1126-6708/2007/11/070, arXiv:0709.2092.
- [57] S. Alioli, P. Nason, C. Oleari, and E. Re, “A general framework for implementing NLO calculations in shower Monte Carlo programs: the POWHEG BOX”, *JHEP* **06** (2010) 043, doi:10.1007/JHEP06(2010)043, arXiv:1002.2581.
- [58] K. Hamilton, P. Nason, and G. Zanderighi, “MINLO: Multi-scale improved NLO”, *JHEP* **10** (2012) 155, doi:10.1007/JHEP10(2012)155, arXiv:1206.3572.
- [59] G. Luisoni, P. Nason, C. Oleari, and F. Tramontano, “ $HW^\pm/HZ + 0$ and 1 jet at NLO with the POWHEG BOX interfaced to GoSam and their merging within MiNLO”, *JHEP* **10** (2013) 083, doi:10.1007/JHEP10(2013)083, arXiv:1306.2542.
- [60] LHC Higgs Cross Section Working Group, “Handbook of LHC Higgs cross sections: 4. deciphering the nature of the Higgs sector”, *CERN* (2016) doi:10.23731/CYRM-2017-002, arXiv:1610.07922.
- [61] G. Ferrera, M. Grazzini, and F. Tramontano, “Higher-order QCD effects for associated WH production and decay at the LHC”, *JHEP* **04** (2014) 039, doi:10.1007/JHEP04(2014)039, arXiv:1312.1669.
- [62] G. Ferrera, M. Grazzini, and F. Tramontano, “Associated ZH production at hadron colliders: the fully differential NNLO QCD calculation”, *Phys. Lett. B* **740** (2015) 51, doi:10.1016/j.physletb.2014.11.040, arXiv:1407.4747.
- [63] G. Ferrera, M. Grazzini, and F. Tramontano, “Associated WH production at hadron colliders: a fully exclusive QCD calculation at NNLO”, *Phys. Rev. Lett.* **107** (2011) 152003, doi:10.1103/PhysRevLett.107.152003, arXiv:1107.1164.
- [64] G. Ferrera, G. Somogyi, and F. Tramontano, “Associated production of a Higgs boson decaying into bottom quarks at the LHC in full NNLO QCD”, *Phys. Lett. B* **780** (2018) 346, doi:10.1016/j.physletb.2018.03.021, arXiv:1705.10304.
- [65] O. Brein, R. V. Harlander, and T. J. E. Zirke, “vh@nnlo — Higgs Strahlung at hadron colliders”, *Comput. Phys. Commun.* **184** (2013) 998, doi:10.1016/j.cpc.2012.11.002, arXiv:1210.5347.

-
- [66] R. V. Harlander, S. Liebler, and T. Zirke, “Higgs Strahlung at the Large Hadron Collider in the 2-Higgs-doublet model”, *JHEP* **02** (2014) 023, doi:10.1007/JHEP02(2014)023, arXiv:1307.8122.
- [67] A. Denner, S. Dittmaier, S. Kallweit, and A. Mück, “HAWK 2.0: A Monte Carlo program for Higgs production in vector-boson fusion and Higgs strahlung at hadron colliders”, *Comput. Phys. Commun.* **195** (2015) 161, doi:10.1016/j.cpc.2015.04.021, arXiv:1412.5390.
- [68] J. Alwall et al., “The automated computation of tree-level and next-to-leading order differential cross sections, and their matching to parton shower simulations”, *JHEP* **07** (2014) 079, doi:10.1007/JHEP07(2014)079, arXiv:1405.0301.
- [69] S. Frixione, P. Nason, and G. Ridolfi, “A positive-weight next-to-leading-order Monte Carlo for heavy flavour hadroproduction”, *JHEP* **09** (2007) 126, doi:10.1088/1126-6708/2007/09/126, arXiv:0707.3088.
- [70] E. Re, “Single-top Wt-channel production matched with parton showers using the POWHEG method”, *Eur. Phys. J. C* **71** (2011) 1547, doi:10.1140/epjc/s10052-011-1547-z, arXiv:1009.2450.
- [71] R. Frederix, E. Re, and P. Torrielli, “Single-top t -channel hadroproduction in the four-flavour scheme with POWHEG and aMC@NLO”, *JHEP* **09** (2012) 130, doi:10.1007/JHEP09(2012)130, arXiv:1207.5391.
- [72] S. Alioli, P. Nason, C. Oleari, and E. Re, “NLO single-top production matched with shower in POWHEG: s - and t -channel contributions”, *JHEP* **09** (2009) 111, doi:10.1088/1126-6708/2009/09/111, arXiv:0907.4076. [Erratum: doi:10.1007/JHEP02(2010)011].
- [73] M. Czakon and A. Mitov, “Top++: A program for the calculation of the top-pair cross-section at hadron colliders”, *Comput. Phys. Commun.* **185** (2014) 2930, doi:10.1016/j.cpc.2014.06.021, arXiv:1112.5675.
- [74] M. Czakon et al., “Top-pair production at the LHC through NNLO QCD and NLO EW”, *JHEP* **10** (2017) 186, doi:10.1007/JHEP10(2017)186, arXiv:1705.04105.
- [75] T. Melia, P. Nason, R. Rontsch, and G. Zanderighi, “ W^+W^- , WZ and ZZ production in the POWHEG BOX”, *JHEP* **11** (2011) 078, doi:10.1007/JHEP11(2011)078, arXiv:1107.5051.
- [76] M. Grazzini et al., “NNLO QCD + NLO EW with Matrix+OpenLoops: precise predictions for vector-boson pair production”, *JHEP* **02** (2020) 087, doi:10.1007/JHEP02(2020)087, arXiv:1912.00068.
- [77] NNPDF Collaboration, “Parton distributions for the LHC Run II”, *JHEP* **04** (2015) 040, doi:10.1007/JHEP04(2015)040, arXiv:1410.8849.
- [78] NNPDF Collaboration, “Parton distributions from high-precision collider data”, *Eur. Phys. J. C* **77** (2017) 663, doi:10.1140/epjc/s10052-017-5199-5, arXiv:1706.00428.
- [79] T. Sjöstrand et al., “An introduction to PYTHIA 8.2”, *Comput. Phys. Commun.* **191** (2015) 159, doi:10.1016/j.cpc.2015.01.024, arXiv:1410.3012.

- [80] CMS Collaboration, “Event generator tunes obtained from underlying event and multiparton scattering measurements”, *Eur. Phys. J. C* **76** (2016) 155, doi:10.1140/epjc/s10052-016-3988-x, arXiv:1512.00815.
- [81] CMS Collaboration, “Extraction and validation of a new set of CMS PYTHIA8 tunes from underlying-event measurements”, *Eur. Phys. J. C* **80** (2020) 4, doi:10.1140/epjc/s10052-019-7499-4, arXiv:1903.12179.
- [82] R. Frederix and S. Frixione, “Merging meets matching in MC@NLO”, *JHEP* **12** (2012) 061, doi:10.1007/JHEP12(2012)061, arXiv:1209.6215.
- [83] J. Alwall et al., “Comparative study of various algorithms for the merging of parton showers and matrix elements in hadronic collisions”, *Eur. Phys. J. C* **53** (2008) 473, doi:10.1140/epjc/s10052-007-0490-5, arXiv:0706.2569.
- [84] T. Plehn, G. P. Salam, and M. Spannowsky, “Fat jets for a light Higgs”, *Phys. Rev. Lett.* **104** (2010) 111801, doi:10.1103/PhysRevLett.104.111801, arXiv:0910.5472.
- [85] Y. Wang et al., “Dynamic Graph CNN for learning on point clouds”, *ACM Trans. Graph.* **38** (2019) 146, doi:10.1145/3326362, arXiv:1801.07829.
- [86] CMS Collaboration, “Identification of highly Lorentz-boosted heavy particles using graph neural networks and new mass decorrelation techniques”, CMS Detector Performance Note CMS-DP-2020-002, 2020.
- [87] A. Butter et al., “The machine learning landscape of top taggers”, *SciPost Phys.* **7** (2019) 014, doi:10.21468/SciPostPhys.7.1.014, arXiv:1902.09914.
- [88] CMS Collaboration, “Identification of heavy, energetic, hadronically decaying particles using machine-learning techniques”, *JINST* **15** (2020) P06005, doi:10.1088/1748-0221/15/06/P06005, arXiv:2004.08262.
- [89] CMS Collaboration, “Calibration of the mass-decorrelated ParticleNet tagger for boosted $b\bar{b}$ and $c\bar{c}$ jets using LHC Run 2 data”, CMS Detector Performance Note CMS-DP-2022-005, 2022.
- [90] E. Bols et al., “Jet flavour classification using DeepJet”, *JINST* **15** (2020) P12012, doi:10.1088/1748-0221/15/12/P12012, arXiv:2008.10519.
- [91] CMS Collaboration, “Performance of the DeepJet b tagging algorithm using 41.9/fb of data from proton-proton collisions at 13 TeV with Phase 1 CMS detector”, CMS Detector Performance Note CMS-DP-2018-058, 2018.
- [92] CMS Collaboration, “A new calibration method for charm jet identification validated with proton-proton collision events at $\sqrt{s} = 13$ TeV”, *JINST* **17** (2022) P03014, doi:10.1088/1748-0221/17/03/P03014, arXiv:2111.03027.
- [93] CMS Collaboration, “A deep neural network for simultaneous estimation of b jet energy and resolution”, *Comput. Softw. Big Sci.* **4** (2020) 10, doi:10.1007/s41781-020-00041-z, arXiv:1912.06046.
- [94] CMS Collaboration, “Observation of Higgs boson decay to bottom quarks”, *Phys. Rev. Lett.* **121** (2018) 121801, doi:10.1103/PhysRevLett.121.121801, arXiv:1808.08242.

- [95] ATLAS and CMS Collaborations, and the LHC Higgs Combination Group, “Procedure for the LHC Higgs boson search combination in Summer 2011”, Technical Report CMS-NOTE-2011-005, ATL-PHYS-PUB-2011-11, 2011.
- [96] G. Cowan, K. Cranmer, E. Gross, and O. Vitells, “Asymptotic formulae for likelihood-based tests of new physics”, *Eur. Phys. J. C* **71** (2011) 1554, doi:10.1140/epjc/s10052-011-1554-0, arXiv:1007.1727. [Erratum: doi:10.1140/epjc/s10052-013-2501-z].
- [97] T. Junk, “Confidence level computation for combining searches with small statistics”, *Nucl. Instrum. Meth. A* **434** (1999) 435, doi:10.1016/S0168-9002(99)00498-2, arXiv:hep-ex/9902006.
- [98] A. L. Read, “Presentation of search results: The CL_s technique”, *J. Phys. G* **28** (2002) 2693, doi:10.1088/0954-3899/28/10/313.
- [99] “HEPData record for this analysis”, 2022. doi:10.17182/hepdata.128675.
- [100] LHC Higgs Cross Section Working Group, “Handbook of LHC Higgs cross sections: 3. Higgs properties”, CERN Yellow Report CERN-2013-004, 2013. doi:10.5170/CERN-2013-004, arXiv:1307.1347.